

Phonon-Assisted Electroluminescence from Metallic Carbon Nanotubes and Graphene

S. Essig,^{†,‡} C. W. Marquardt,^{†,‡} A. Vijayaraghavan,[†] M. Ganzhorn,^{†,‡} S. Dehm,[†] F. Hennrich,[†] F. Ou,[§] A. A. Green,^{||} C. Sciascia,[∇] F. Bonaccorso,[∇] K.-P. Bohnen,[⊥] H. v. Löhneysen,^{‡,⊥,⊙} M. M. Kappes,^{#,⊙} P. M. Ajayan,[§] M. C. Hersam,^{||} A. C. Ferrari,[∇] and R. Krupke^{*,†,⊙}

[†]Institut für Nanotechnologie, Karlsruhe Institute of Technology, 76021 Karlsruhe, Germany, [‡]Physikalisches Institut, Karlsruhe Institute of Technology, 76128 Karlsruhe, Germany, [§]Department of Mechanical Engineering & Materials Science, Rice University, Houston, Texas 77005, ^{||}Department of Materials Science and Engineering, Northwestern University, Evanston, Illinois 60208-3108, [⊥]Institut für Festkörperphysik, Karlsruhe Institute of Technology, 76021 Karlsruhe, Germany, [#]Institut für Physikalische Chemie, Karlsruhe Institute of Technology, 76128 Karlsruhe, Germany, [∇]Department of Engineering, University of Cambridge, Cambridge CB3 0FA, United Kingdom, and [⊙]DFG Center for Functional Nanostructures (CFN), 76028 Karlsruhe, Germany

ABSTRACT We report on light emission from biased metallic single-wall carbon nanotube (SWNT), multiwall carbon nanotube (MWNT) and few-layer graphene (FLG) devices. SWNT devices were assembled from tubes with different diameters in the range 0.7–1.5 nm. They emit light in the visible spectrum with peaks at 1.4 and 1.8 eV. Similar peaks are observed for MWNT and FLG devices. We propose that this light emission is due to phonon-assisted radiative decay from populated π^* band states at the M point to the Fermi level at the K point. Since for most carbon nanotubes as well as for graphene the energy of unoccupied states at the M point is close to 1.6 eV, the observation of two emission peaks at $\sim 1.6 \pm \sim 0.2$ eV could indicate radiative decay under emission or absorption of optical phonons, respectively.

KEYWORDS Carbon nanotubes, graphene, electroluminescence, phonons

INTRODUCTION

Single-wall carbon nanotubes (SWNT) have a unique structure–property correlation, yielding electronic properties that depend on the diameter and chiral angle.¹ This correlation not only determines the electrical response of SWNTs in transport measurements,² but also their optical response in absorption, Raman, and fluorescence spectroscopies.^{3–5} In most experiments those responses have been studied separately, and only in recent years, photoconductivity and electroluminescence experiments have been reported.^{6–8} Such measurements study the absorption and emission of photons in SWNT devices under bias and form the basis for a future nanotube-based optoelectronics. It is generally accepted that photoconductivity in SWNT devices is caused by the generation and dissociation of excitons at the nanotube-metal contact.^{6,7} Electroluminescence, the inverse process, has been reported in ref 8 on an ambipolar semiconducting SWNT device, where excitons are formed by injection of electrons and holes. The emission peak in the near-infrared (NIR) range was assigned to a radiative decay over the first interband transition of the π bands at the K point.⁸ Later it was shown in refs 9 and 10 that, under very large bias, impact ionization sets in as a mechanism for exciton formation in unipolar

devices. A comparison between electroluminescence and fluorescence spectra provided evidence for the validity of the proposed model for semiconducting SWNTs.^{9,10} Somewhat unexpected was the observation of electroluminescence from biased metallic SWNTs, reported first in ref 11 and later in ref 12, because fluorescence of metallic SWNTs has not been observed so far. The proposed mechanism is based on thermal population and depopulation of states at the van Hove singularities close to the K point.¹¹ Radiative recombination could then occur via the corresponding interband transition. Within this model, the emitted photon energy scales inversely with nanotube diameter.¹¹

Here we study the current-induced light emission from metallic SWNTs with different diameters ranging from 0.7 to 1.5 nm, and report a universal, diameter independent, light emission in the visible part of the spectrum. The data is complemented by measurements on multiwall carbon nanotube (MWNT) and few-layer graphene (FLG) devices. We assign the electroluminescence to phonon-assisted radiative decay from π^* band states at the M point to the Fermi level at the K point.

Experimental Section. The devices were produced by combining density gradient ultracentrifugation (DGU) or gel filtration (GF) sorting of SWNTs, MWNTs, and FLGs, with dielectrophoretic (DEP) assembling from dispersion. The details to the DGU, GF sorting, and DEP assembling can be found in refs 13–16. We used SWNTs from three dispersions with tubes of various diameters d , as measured by

* To whom correspondence should be addressed. E-mail: ralph.krupke@kit.edu.

Received for review: 11/30/2009

Published on Web: 04/20/2010



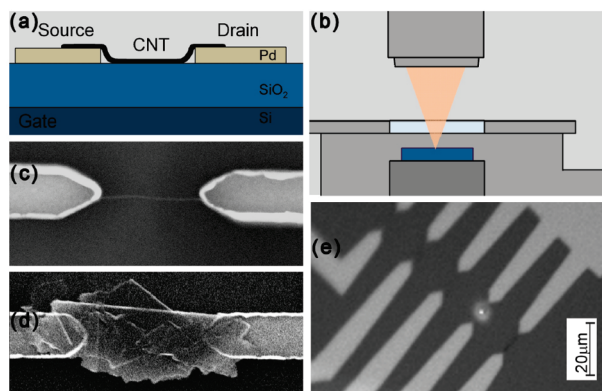


FIGURE 1. (a) Cross-Sectional schematic of the device geometry, and (b) of the sample in the optical cryostat, from which the emitted light is coupled into the microscope and spectrometer. Scanning electron micrograph of (c) SWNT device, and (d) FLG device. (e) Optical image of a device array, overlaid with the electroluminescence signal from a biased SWNT contact.

absorption spectroscopy. Dispersion SWNT#A, produced by DGU of pulsed-laser-vaporization material in aqueous sodium cholate solution, contains large-diameter metallic SWNTs with $d = 1.49 - 0.94$ nm (Figure S1a). Dispersion SWNT#B, produced by GF of CoMoCat material in aqueous sodium dodecyl sulfonate solution, contains medium-diameter metallic SWNTs with $d = 0.98 - 0.87$ nm (Figure S1b). The third dispersion SWNT#C, produced by DGU of CoMoCat material in aqueous sodium cholate solution, contains small-diameter metallic SWNTs of two chiralities (6,6) and (7,4), with $d = 0.83$ and 0.77 nm, respectively (Figure S1c). Although SWNT#C contains (6,5) and other semiconducting nanotubes, we have assembled only the metallic species by choosing the appropriate DEP conditions.¹⁷ This is confirmed by the nearly linear current–voltage characteristics and the absence of significant gate-voltage dependence in all devices (Figure S2). Dispersion FLG#D contains few-layer graphene flakes in N,N-dimethylacetamide, produced by liquid phase exfoliation of graphite via sonication followed by an ultracentrifugation step.¹⁸ Dispersion MWNT#E contains MWNTs in aqueous sodium cholate with $d = 60$ nm, produced by dissolution of the alumina template, in which the MWNTs were grown without transition element catalyst.¹⁹ All dispersions were diluted with the respective solvent to a carbon concentration of ~ 400 ng/mL prior to deposition.

Arrays of CNT and FLG devices were prepared by dielectrophoretic deposition onto Pd(40 nm)/Ti(5 nm) electrodes on p-doped (100)-Si substrates ($<0.001 \Omega\text{cm}$) with an 800 or 1000 nm thermal SiO₂ layer, and on Au(40 nm)/Cr(5 nm) electrodes on (c-plane)-Al₂O₃ substrates (Figure 1a). Electrodes were defined by electron beam lithography and metal sputtering, with gap sizes of 750 nm for SWNT and FLG devices and 10 μm for MWNT devices. The optimum DEP assembling frequency f and peak-to-peak voltage V_{pp} were determined by voltage-contrast scanning electron microscopy (VC-SEM)²⁰ and are $f = 300$ kHz to 3 MHz and $V_{pp} =$

1.2–1.6 V for SWNTs and FLGs, and $f = 300$ kHz and $V_{pp} = 15$ V for MWNTs. The wire-bonded samples were mounted via a ceramic package in an Oxford HiRes optical cryostat (Figure 1b), and electrically connected to an Agilent 4155C semiconductor parameter analyzer. The optical window of the cryostat allows us to locate the light emitting device and to analyze the light spectrum, by guiding the light through a Zeiss AxioTech Vario microscope (objective 40 \times , NA = 0.6) to an Acton SpectraPro 2150i spectrograph. In the spectrograph, the light is either reflected by a mirror or diffracted by a grating (750 nm blaze, 300 grooves/mm), before it reaches a Pixis 256E CCD Si detector. The dark current of the CCD detector yields about 2 counts per pixel per hour, and allows integrating the signal over extended periods. The typical integration time in this experiment is up to 20 min. We estimate the sensitivity of the setup on the basis of the quantum efficiency and amplifier gain of the CCD, the efficiency of the grating, the geometrical constraints of the microscope optics (optical path), and by assuming an isotropic emitter. The sensitivity s is about 10^5 and 10^5 emitted photons per count, in reflection and diffraction mode, respectively, and the bandwidth per pixel $\Delta\lambda$ is 0.5 nm. The relative spectral response of the system has been measured by a calibrated halogen lamp and all recorded spectra were corrected accordingly. The spatial and spectral resolution are 0.7 μm and 1.5 nm, respectively. The measurements were done under vacuum at a base pressure of $<10^{-6}$ mbar.

Results and Discussion. SEM images of SWNT and FLG devices are shown in Figure 1, panels c and d. The source and drain electrodes are typically bridged by 1–5 SWNTs, one FLG or one MWNT. Figure 1e is a reflection mode image of a SWNT#A array with five devices under external illumination, overlaid with an image recorded without illumination. The bright spot is caused by electroluminescence of device 4 under source-drain bias. Figure 2a shows the spectra of the emitted light and their evolution with increasing bias voltage, typical for SWNT#A devices. From the measured intensity I in units of counts per second we have calculated the spectral photon flux $dn/(dt dE)$ in units of photons per second and electronvolt

$$\frac{dn}{dt dE} = I \frac{s}{\Delta\lambda E^2} \quad (1)$$

where s is the sensitivity in the diffraction mode, $\Delta\lambda$ the bandwidth, E the energy E in eV, c the speed of light, and h the Planck constant in eV \cdot s. The spectra can be deconvoluted in two Gaussians centered at ~ 1.35 and ~ 1.76 eV, with a full width at half-maximum (FWHM) of 0.28 and 0.24 eV, respectively. The peak position and FWHM change weakly with the applied voltage (Figure 4), but the peak intensity increases exponentially with the voltage (Figure 5a).

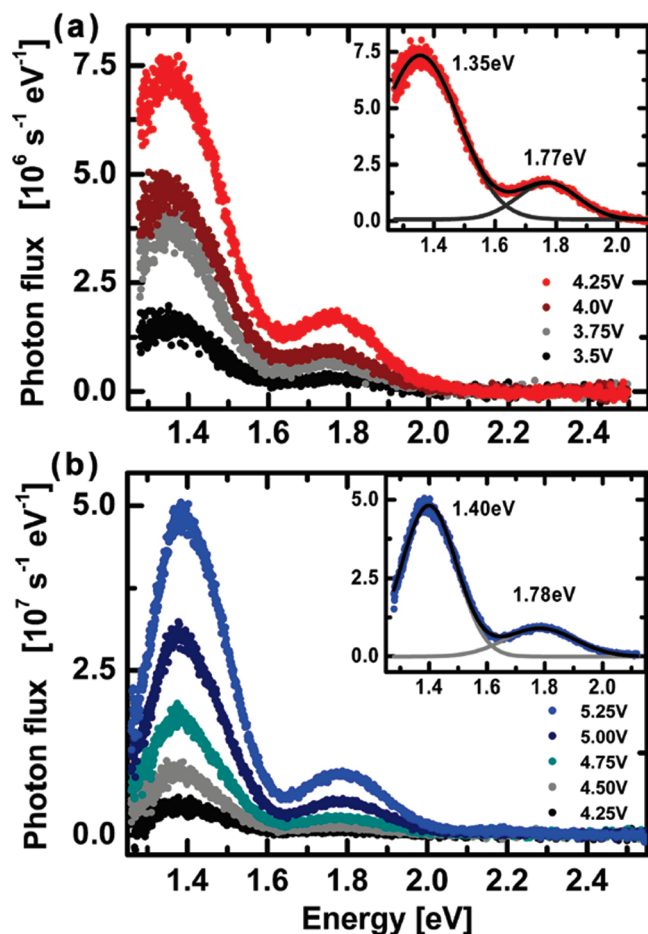


FIGURE 2. Electroluminescence spectra of devices prepared from (a) large diameter ($d = 1.49\text{--}0.94$ nm) SWNT#A tubes and (b) from medium diameter ($d = 0.98\text{--}0.87$ nm) SWNT#B tubes. Indicated are traces with increasing source-drain voltage V_{SD} . Insets show the Gaussian fits to the uppermost trace with the fitted peak positions.

To the best of our knowledge, the appearance of two emission peaks for SWNTs under source-drain bias, in the energy range 1.3–2.5 eV, was not discussed before. We note, however, that ref 21 reported emission with nearly identical peaks in position and FWHM, induced by electron tunnelling from a scanning tunnelling microscope tip into MWNTs. Ref 21 assigned the two peaks to E_{44} and E_{55} transitions, which are diameter dependent transitions at the K point in the electronic band structure. However, they did not report variations in the double-peak position, despite the range of MWNT diameters investigated (7–12 nm). Likewise, in our SWNT#A devices, with $d = 1.49\text{--}0.94$ nm, we do not observe significant changes in the spectra for different devices, and we cannot identify a pair of transition energies that could fit the observed peak positions.²² Splitting of transition energies due to trigonal warping²³ could qualitatively explain the double-structure in non-armchair metallic SWNTs. However, the trigonal-warping induced splitting for the SWNT#A tubes, expected in the range of 0.2–0.3 eV,²³ is too small compared to the observed energy difference ΔE

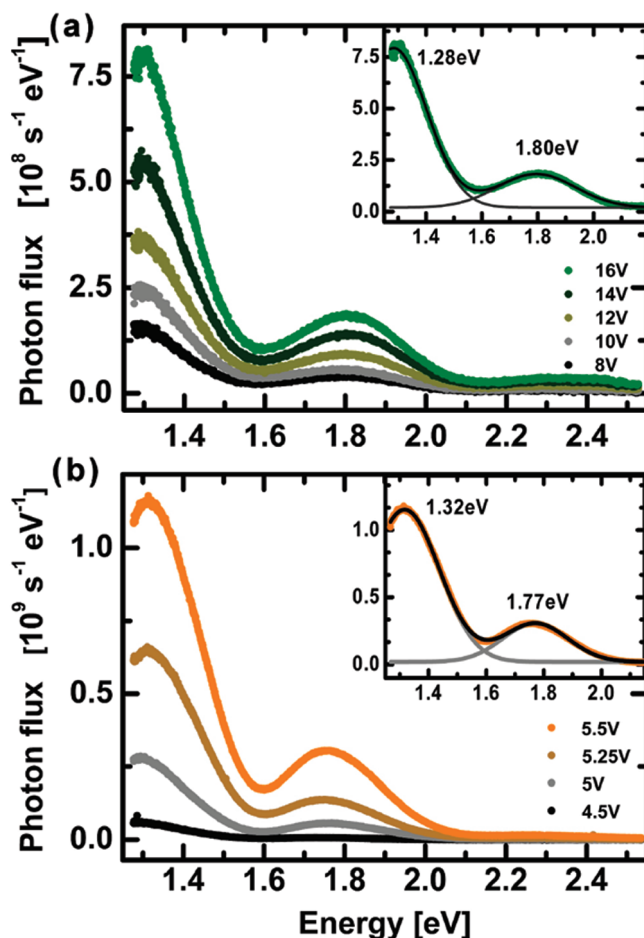


FIGURE 3. Electroluminescence spectra of devices prepared from (a) small diameter ($d = 0.83$ nm, 0.77 nm) (6,6) or (7,4) SWNT#C tubes and (b) from few-layer graphene FLG#D flakes. Indicated are traces with increasing source-drain voltage V_{SD} . Insets show the Gaussian fits to the uppermost trace with the fitted peak positions.

≈ 0.4 eV of the two emission peaks. To explore the sensitivity of the spectra to tube diameter, we measured light emission from SWNT#B devices with $d = 0.98\text{--}0.87$ nm. Again the spectra are composed of two peaks, centered at ~ 1.39 and ~ 1.77 eV with a FWHM of ~ 0.23 and ~ 0.29 eV, respectively (Figure 2b). The peak intensity increases with voltage (Figure 5). Hence the spectra for the medium-diameter SWNTs are very similar to those of larger-diameter SWNTs. We note that, if we assigned the peaks as K-point interband transitions, for 0.87–0.98 nm diameter tubes, the trigonal warping-induced splitting would be $\Delta E \approx 0.5$ eV,²³ but the lowest transition energy E_{11} would be at ~ 2.5 eV, by far exceeding our peak energies.

Thus, the two emission peaks in the 1.3–2.5 eV range do not depend on SWNT diameter and are not related to K-point interband transitions. This is further supported by measurements on SWNT#C devices from (7,4) and (6,6) tubes, with $d = 0.83$ and 0.77 nm, respectively. The emission peak positions are slightly shifted to ~ 1.28 and ~ 1.79 eV, with FWHM of ~ 0.28 and ~ 0.33 eV (Figure 3a), and the

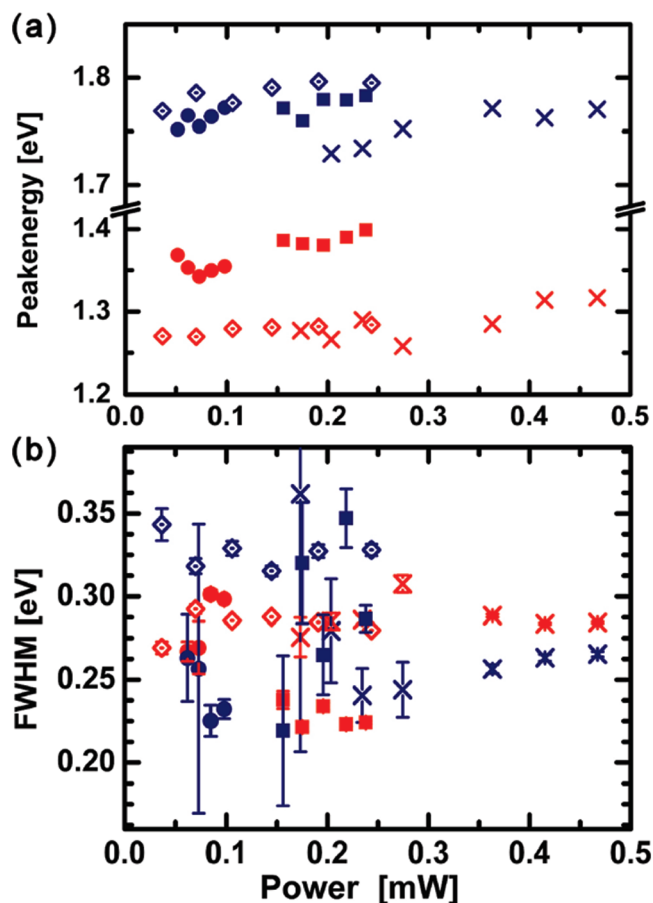


FIGURE 4. (a) Emission peak positions, and (b) widths of SWNT#A (blue circle, red circle), SWNT#B (blue square, red square), SWNT#C (blue dotted diamond, red dotted diamond), and FLG#D (blue \times , red \times) devices versus electric power. The blue and red symbols denote the high and low energy emission peaks, respectively.

intensity again increases with voltage (Figure 5). For these small-diameter SWNTs, E_{11} is at ~ 3 eV, too large to match the emission peak energies.

Before discussing the intrinsic origin of the peaks we note that the Si/SiO₂ substrate and the Ti/Pd electrodes can be excluded as other direct or indirect light sources. Devices prepared on Al₂O₃ with Au/Cr or Ti/Pd electrodes show similar emission peaks (Figure S3a,b). Likewise, an effect of catalyst impurities can be excluded, since we measured similar spectra on devices with MWNTs grown without transition-element catalyst (MWNT#E, Figure S3c). In addition, we observed that controlled oxidation with meta-chloroperbenzoic acid (MCPBA)²⁴ does not increase the emission intensity, which indicates that oxygen or oxygen-induced defects are unlikely to be important (Figure S4).

We therefore conclude that the emission at ~ 1.4 and ~ 1.8 eV originate from the carbon nanotubes. At the same time, the peak positions do not scale with tube diameter, which is inconsistent with K-point interband transitions as origin of the emissions.²⁵ However, electronic states in the relevant energy range that do not significantly depend on the nanotube diameter do exist, and these are the π^* and π

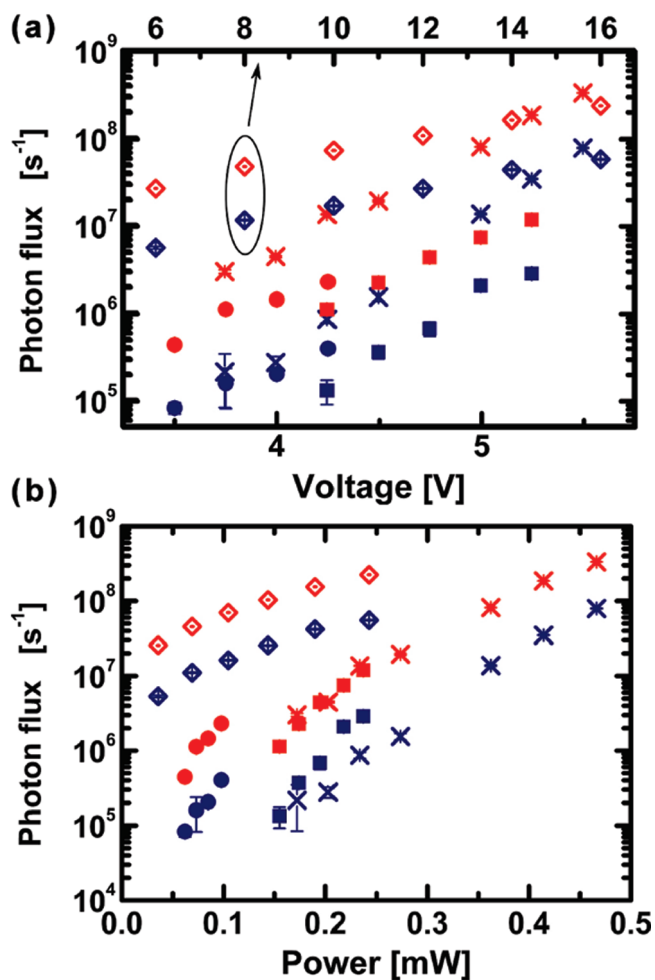


FIGURE 5. Integrated photon flux versus (a) voltage, and (b) power of SWNT#A (blue circle, red circle), SWNT#B (blue square, red square), SWNT#C (blue dotted diamond, red dotted diamond), and FLG#D (blue \times , red \times) devices versus electric power. The blue and red symbols denote the high and low energy emission peaks, respectively.

bands at the M point. For graphene, the single-particle excitation states are calculated to be 1.6 and 2.3 eV above and below the Fermi level, respectively.²⁶ In SWNTs, the bands split due to confinement, but the energies of the bottom of the conduction band and the top of the valence band at the M point are for most SWNTs close to the values for graphene.^{26–28} It is thus tempting to associate the emission with the energy of the π^* states at the M point, populated under large bias. Indeed a high-density of unoccupied states at ~ 1.7 eV on graphite has been measured by inverse photo emission and tunnelling spectroscopy.²⁹ In our experiment, the radiative decay from those states at the M point to the Fermi level at the K point requires scattering with a high-momentum optical phonon, in order to satisfy momentum conservation (Figure 6). Phonon-assisted emission from the M-point states would then explain the observation of two peaks at $\sim 1.6 \pm 0.2$ eV, and $\Delta E/2 \sim 0.2$ eV would be a measure for the phonon energy.

Anticipating that similar emission peaks should be observable in graphene as well, we studied light emission from

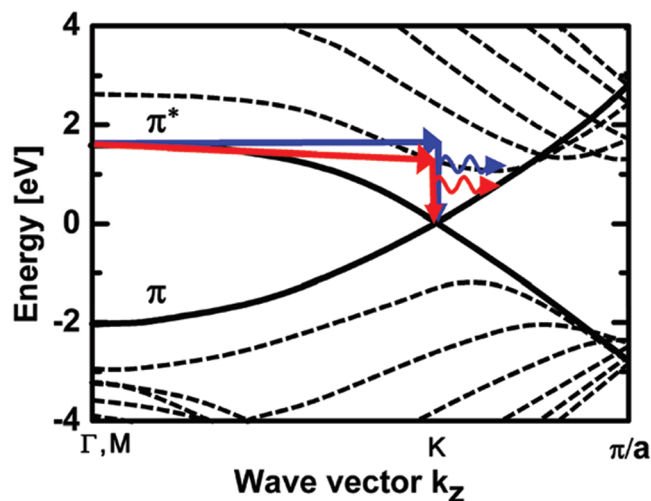


FIGURE 6. Electronic band structure of a (6,6) SWNT [adapted from ref 27]. The dashed lines indicate the one-dimensional π and π^* bands. The full line indicates the $m = 0,6$ bands, and are similar to the graphene dispersion. The energies of these two bands at the M point are similar for most SWNTs.²⁶ The proposed mechanism of light emission due to phonon-assisted radiative decay from populated π^* band states at the M point to the Fermi level at the K point is indicated by the color arrows. Emission of higher (blue wavy arrow) and lower (red wavy arrow) energetic photons is mediated by the absorption (straight blue arrow) and emission (straight red arrow) of high-energy, high-momentum phonons.

FLG#D devices (Figure 3b). Indeed emission peaks at ~ 1.29 and ~ 1.74 eV, with FWHM of ~ 0.29 and ~ 0.27 eV, are observed, and the intensities increase with the voltage. In FLG devices we could study the peak positions and widths over a wider power range, and noticed a small increase in the positions by ~ 0.2 eV/mW (Figure 4a), along with a convergence of the peak widths to ~ 0.28 eV (Figure 4b).

To identify the phonon involved, we argue that the momentum for the electronic transition from M to K has to be provided by a phonon in the Γ –K direction with momentum $\leq 0.5|\Gamma K|$ (Figure 7a,b). Within this momentum range it is the longitudinal optical (LO) branch which is closest to $\Delta E/2 \approx 0.2$ eV, and hence most likely can provide the phonons involved in the emission process, while the TO branch with ~ 0.17 eV at a wave vector $0.5|\Gamma K|$ is only slightly lower in energy. The electron–phonon coupling (EPC) of those branches depends strongly on the position of the Fermi level E_F with respect to the charge neutrality point E_0 . At $E_F = E_0$, the EPC for the LO and TO phonons is large only at the Γ and K points, respectively.³⁰ For $E_F \neq E_0$, which we assume is the situation imposed by the very large source-drain bias in our experiment, a significant EPC for both phonon branches extends from Γ and K, although midway between Γ and K, EPC is still zero for both modes at the doping level considered theoretically.^{31,32} It is, however, conceivable that for $E_F \gg E_0$ a sizable EPC develops around $0.5|\Gamma K|$. Detailed EPC calculations of the LO and TO phonons for $E_F \gg E_0$ along the Γ –K direction under non-equilibrium conditions are needed to fully model our experimental findings. As for SWNTs we have also to consider

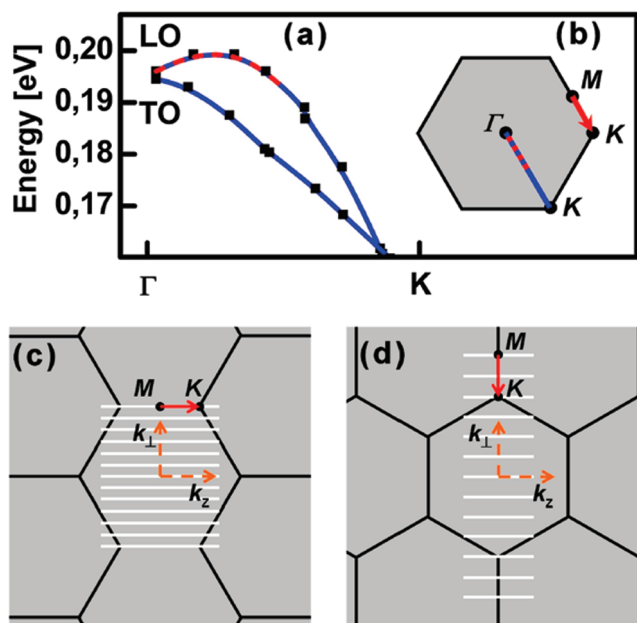


FIGURE 7. (a) Phonon dispersions of graphite along the Γ –K direction. (b) Brillouin zone of graphite with the high-symmetry points Γ , K, and M. The momentum for the electronic transition from M to K (red arrow), is provided by phonons in the Γ –K direction (blue line). In the relevant momentum range (red dashes), phonons of the LO branch have energy consistent with that required to explain the electroluminescence data. In armchair-type metallic SWNTs like the (6,6) in (c), and in zigzag-type metallic SWNT like the (9,0) in (d), phonons have to provide the momentum in the k_z and k_{\perp} direction, respectively. Data points in (a) from Ref 39.

that, with respect to k_F , metallic carbon nanotubes belong to two classes:³³ The first class comprises armchair SWNTs, and chiral SWNTs with $n - m = 3pG$; n, m are the SWNT indices, G is the largest common denominator of n and m , and p is an integer. We refer to them as armchair-type metallic tubes, which have an electronic band structure similar to Figure 6. In these tubes, states at the M and K point differ in momentum along the nanotube axis Δk_z , and the transition requires the identified phonon (Figure 7c). The second class comprises zigzag SWNTs, and chiral SWNTs with $n - m \neq 3pG$; referred to as zigzag-type metallic SWNTs. In these tubes, states at the M and K point differ in momentum along the circumference Δk_{\perp} , perpendicular to the nanotube axis, and in these cases a phonon as well is required for the transition (Figure 7d). Hence this model can account for the two emission lines in graphene and in metallic carbon nanotubes.

From our experiments, the two emission peaks in the range 1.3–2.5 eV appear to be universal to substrate-supported metallic nanotube and graphene devices under bias. The measurements of ref 21 on MWNTs are consistent with this hypothesis. Reference 12 also reported two emission lines from a $d = 2.3$ nm metallic SWNT device, albeit in the NIR range. They assigned a peak at ~ 1.04 eV to E_{11} K-point interband transitions, and a second peak at ~ 0.87 eV to phonon-assisted E_{11} emission. It is not clear what the relation between these NIR peaks and our measurements

is. However, we would like to remark that the 1.8 and 1.4 eV emission could appear as second-orders at ~ 0.9 and ~ 0.7 eV in the NIR spectra.³⁴ Interestingly ref 12 reported that the ~ 0.87 eV peak is only observed on substrate-supported SWNT segments but not on suspended ones. Likewise ref 11 did not report a double peak from suspended SWNTs. Thus, it seems that a double peak is only observed on the substrate-supported devices, but does not depend on the substrate material. We observed the two peaks from devices on SiO₂ and Al₂O₃ substrates, and ref 21 reported these for a HOPG substrate, while ref 12 measured two peaks in the NIR range on devices on Si₃N₄. An evident difference between experiments on supported and suspended tubes is that substrate-supported tubes can sustain more than 1 order of magnitude higher electrical power than suspended ones. At the same time Joule heating is suppressed due to substrate cooling, resulting in the absence of thermal radiation in our data as well as in ref 12. However, although the nanotube temperature remains low, the LO phonon population will be significantly enhanced under large bias,^{35,36} and thus enable the phonon-absorption-assisted second emission peak at higher energy. We also notice that in all of our substrate-supported devices the electroluminescence intensity increases exponentially with applied voltage (Figure 5a,b), and not with the power as in suspended nanotubes.¹¹ We therefore conclude that the π^* band states at the M point get populated with electrons due to direct carrier injection rather than thermal excitation.

Finally we estimate the power efficiency $\eta = P_{\text{phot}}/P_{\text{el}}$ of the electroluminescence process. We calculate the emitted light power P_{phot} of the two emission peaks as:

$$P_{\text{phot}} = \int \frac{dn}{dt} eE dE \quad (2)$$

and using Gaussian fits for the spectral photon flux. The electrical power P_{el} is obtained from current–voltage curves. We get $\eta = 10^{-8}$ – 10^{-7} for our metallic SWNT and FLG devices, which is about 2–3 orders of magnitude lower than for semiconducting SWNTs.⁹ The emission from semiconducting SWNTs is due to a direct transition, in contrast to the indirect transition in metallic SWNTs reported here. The factor of 10^2 – 10^3 is typical of the efficiencies of direct and indirect semiconductors, cf. $\sim 10^{-7}$ for the indirect semiconductor GaP and $\sim 10^{-5}$ for the direct semiconductor GaAs.^{37,38}

In summary, we have shown that two electroluminescence peaks in the energy range 1.3–2.5 eV appear to be universal to substrate-supported metallic nanotube and few-layer graphene. The peak positions are nearly independent of nanotube diameter, which is inconsistent with K-point interband transitions. We propose that light emission is due to phonon-assisted radiative decay from π^* band states at

the M point to the Fermi level at the K point. Since the energy of the bottom of the conduction band at the M point is for most SWNTs close to the value for graphene, we anticipate that the $\sim 1.6 \pm \sim 0.2$ eV emissions could be general features of substrate-supported nanocarbons.

Acknowledgment. The authors acknowledge D. Resasco for generous donation of CoMoCat raw material, M. Lazzeri and S. Lebedkin, F. Giustino for helpful discussions, and S. Pieke for technical assistance. R.K. acknowledges funding by the Helmholtz-Gemeinschaft Deutscher Forschungszentren (HGF-VH-NG-126), M.C.H. and A.A.G. acknowledge the National Science Foundation (DMR-0520513, EEC-0647560, and DMR-0706067) and the Nanoelectronics Research Initiative, and A.C.F. acknowledges the Royal Society, the European Research Council Grant NANOPOTS, and the EPSRC grant EP/G042357/1.

Supporting Information Available. Optical absorption spectra (S1), device characteristics (S2), and electroluminescence data (S3–S5). This material is available free of charge via the Internet at <http://pubs.acs.org>.

REFERENCES AND NOTES

- (1) Hamada, N.; et al. *Phys. Rev. Lett.* **1992**, *68*, 1579.
- (2) Odom, T. W.; et al. *Nature* **1998**, *391*, 62.
- (3) Fantini, C.; et al. *Phys. Rev. Lett.* **2004**, *93*, 147406.
- (4) O'Connell, M.; et al. *Science* **2002**, *297*, 593.
- (5) Tu, X.; et al. *Nature* **2009**, *460*, 350.
- (6) Freitag, M.; et al. *Nano Lett.* **2003**, *3*, 1067.
- (7) Balasubramanian, K.; et al. *Nano Lett.* **2005**, *5*, 507.
- (8) Misewich, J. A.; et al. *Science* **2003**, *300*, 783.
- (9) Marty, L.; et al. *Phys. Rev. Lett.* **2006**, *96*, 136803.
- (10) Adam, E.; et al. *Nano Lett.* **2008**, *8*, 2351.
- (11) Mann, D.; et al. *Nature Nano* **2007**, *2*, 33.
- (12) Xie, L.; et al. *Nano Lett.* **2009**, *9*, 1747.
- (13) Arnold, M.; et al. *Nature Nano* **2006**, *1*, 60.
- (14) Moshhammer, K.; et al. *Nano Res.* **2009**, *2*, 599.
- (15) Vijayaraghavan, A.; et al. *Nano Lett.* **2007**, *7*, 1556.
- (16) Vijayaraghavan, A. *ACS Nano* **2009**, *3*, 1729.
- (17) Krupke, R.; et al. *Science* **2003**, *301*, 344.
- (18) Hernandez, Y.; et al. *Nat. Nano* **2008**, *3*, 563.
- (19) Ou, F. S.; et al. *Appl. Phys. Lett.* **2006**, *89*, 243122.
- (20) Vijayaraghavan, A.; et al. *Nano Res.* **2008**, *1*, 321.
- (21) Uemura, T. *Surf. Sci.* **2006**, *600*, L15–L19.
- (22) Doorn, S. K.; et al. *Phys. Rev. B* **2008**, *78*, 165408.
- (23) Saito, R.; et al. *Phys. Rev. B* **2000**, *61*, 2981.
- (24) Balch, A.; et al. *J. Am. Chem. Soc.* **1993**, *117*, 8926.
- (25) Mintmire, J. W.; et al. *Phys. Rev. Lett.* **1992**, *68*, 631.
- (26) Reich, S.; et al. *Phys. Rev. B* **2002**, *65*, 155411.
- (27) Reich, S. Ph.D. thesis; Technische Universität: Berlin, 2002.
- (28) Takagi, Y.; et al. *Phys. Rev. B* **2009**, *79*, 233406.
- (29) Reihl, B.; et al. *Phys. Rev. B* **1986**, *33*, 5770.
- (30) Piscanec, S.; et al. *Phys. Rev. Lett.* **2004**, *93*, 185503.
- (31) Park, C.-W.; et al. *Nano Lett.* **2008**, *8*, 4229.
- (32) Basko, D. M.; et al. *Phys. Rev. B* **2009**, *80*, 165413.
- (33) Jishi, R. A.; et al. *J. Phys. Soc. Jpn.* **1994**, *63*, 2252.
- (34) For our samples we have checked that the electroluminescence signal is not of second order (Figure S5).
- (35) Oron-Carl, M.; et al. *Phys. Rev. Lett.* **2008**, *100*, 127401.
- (36) Lazzeri, M.; et al. *Phys. Rev. Lett.* **2005**, *95*, 236802.
- (37) Ivey, H. F. *Electroluminescence and related effects*; Academic Press: New York, 1963.
- (38) Nakano, T.; et al. *Jpn. J. App. Phys.* **1967**, *6*, 665.
- (39) Maultzsch et al., *Phys. Rev. Lett.* **2004**, *92*, 75501.